IEEE Access
Multidisciplinary | Rapid Review | Open Access Journal

Received February 26, 2020, accepted March 16, 2020, date of publication March 31, 2020, date of current version April 16, 2020.

Digital Object Identifier 10.1109/ACCESS.2020.2984515

Real-Time Dynamic Earth-Pressure Regulation Model for Shield Tunneling by Integrating GRU Deep Learning Method With GA Optimization

MIN-YU GAO[1], NING ZHANG[2], SHUI-LONG SHEN[2,3], AND ANNAN ZHOU[3]

[1]Department of Civil Engineering, School of Naval Architecture, Ocean, and Civil Engineering, Shanghai Jiao Tong University, Shanghai 200240, China
[2]Key Laboratory of Intelligence Manufacturing Technology, Ministry of Education, Department of Civil and Environmental Engineering, College of Engineering, Shantou University, Shantou 515063, China
[3]Discipline of Civil and Infrastructure, School of Engineering, Royal Melbourne Institute of Technology, Melbourne, VIC 3001, Australia

Corresponding authors: Ning Zhang (zhangning@stu.edu.cn) and Shui-Long Shen (shensl@stu.edu.cn)

This work was supported in part by the Research Funding of Shantou University for New Faculty Member under Grant NTF19024-2019, in part by the National Nature Science Foundation of China (NSFC) under Grant 41672259, and in part by the Funding for Leadership Talent of Zhujiang Project, Guangdong, in 2019.

ABSTRACT This paper proposes an intelligent framework to predict and automatically regulate earth pressure using a deep learning technique during earth pressure balance shield tunneling. A prediction model was proposed by integrating a new cost function (relative mean square error) with a gated recurrent unit (GRU). The moving average smoothing method was also incorporated into the GRU model to reduce the noise of the dataset and improve the accuracy of the proposed model. A real-time dynamic regulation model for adjusting the operational parameters was proposed by integrating the GRU model into a genetic algorithm-based optimizer. By adjusting the operational parameters, the dynamic regulation model regulates the excessive predicted earth pressure within a suggested range. The proposed prediction and regulation models were applied to a metro tunnel construction in Luoyang, China. The results show that the proposed models provide good guidance for automated tunnel construction.

INDEX TERMS Automatic regulation, earth pressure, gated recurrent unit, genetic algorithm, shield tunneling.

I. INTRODUCTION

Rapid urbanization brings about the large-scale construction of underground infrastructures such as metro lines [1]–[3] and deep excavations [4]. However, issues caused by large-scale construction [5] such as ground settlement [6]–[9], rain-triggered floods [10]–[14], and soil liquefaction [15], [16] lead to significant social, economic, and environmental losses. Several efficient and safe construction techniques have been proposed to solve these issues and mitigate relevant hazards. For one, earth pressure balance (EPB) shield tunneling is widely used in the construction of metro lines because of its minimal disturbance to the environment. During EPB shield tunneling, the excavated materials, when combined with various additives, fill up the soil chamber to provide support pressure to the excavation face [17]. The pressure generally fluctuates because of the dynamic construction of the EPB machine, which disturbs the original soil stress distribution in the ground and thus contributes to ground settlement [18]–[25].

Considering the vital effect of earth pressure at the excavation face to maintain face stability and control ground deformation, the balance of earth pressure has been investigated by mechanical analysis, numerical analysis, and artificial intelligence (AI) technology. Mechanical analysis is mainly based on mechanical equilibrium to calculate earth pressure distribution [26]–[28]. Using numerical simulations such as finite element methods, numerical analysis has been employed to evaluate the relationship between earth pressure and shield operational parameters such as the screw conveyor speed, the advance rate and rotational speed of the cutter head [29], [30]. However, analyses using mechanical and numerical methods have been based mostly on a number of assumptions quite different from the actual construction process. Moreover, current methods cannot be employed to provide a dynamic control of tunnel operational parameters.

The associate editor coordinating the review of this manuscript and approving it for publication was Mustafa Servet Kiran.

Therefore, in recent years, AI methods have been proposed to investigate the earth pressure and automatic control of tunnel operational parameters based on in-situ construction data.

AI technology applied to the field of EPB tunneling mainly uses fuzzy control [31], artificial neural networks [32], [33], random forests [34]–[36], or support vector machines [37]. Fuzzy control has been successfully utilized in the shield tunneling process [38] and improved by hybrid fuzzy control-based methods [39], [40]. However, methods based on fuzzy control rely highly on expert knowledge, fail to tune in a short time, and are less robust. Yeh [41] first applied artificial neural networks to predict earth pressure in a soil chamber and used a grid searching function to find the optimal speeds of the shield jack and screw conveyor. The adaptive neuro-fuzzy inference system (ANFIS) which combines the advantages of fuzzy reasoning and a neural network has been utilized to control earth pressure [42]–[44]. Shi *et al.* [45] used the ANFIS to establish a non-linear mapping between the inputs (real-time monitored thrust, advance-rate and earth pressure) and the outputs (speed of screw conveyor). Li and Shao [46] used the ANFIS to predict the earth pressure of five points on a bulkhead and used the ant colony system algorithm to optimize the speed of the screw conveyor. Liu *et al.* [37] adopted a least squares support vector machine combined with particle swarm optimization to find optimal construction parameters. However, conventional machine learning methods ignore the sequential characteristics of earth pressure owing to the nature of the architecture. Therefore, recurrent neural networks are widely used to consider the sequential characteristics related to tunneling [47]. Gao *et al.* [48] compared different types of recurrent neural network methods and conventional machine learning methods to determine the best model of a gated recurrent unit (GRU) in the prediction of earth pressure. However, existing research on earth pressure has ignored that tunneling construction is a dynamic and sequential problem. Furthermore, the errors that may be contained in the monitored earth pressure are seldom considered when preparing training and test sets.

The objective of this study was to develop a real-time dynamic regulation model (DRM) for operational parameters by integrating a GRU neural network into a genetic algorithm (GA) to dynamically predict the earth pressure during tunneling and recommend optimized operational parameters for an EPB tunneling machine. The paper is organized as follows: following the Introduction, Section II introduces the GRU-based DRM framework and the methodology of the GRU and the GA and defines the different cost functions. Section III introduces the preparation of the datasets, the data smoothing method, and the GRU modelling details. Section IV compares the improved performance of the GRU models with the proposed relative mean square error (REMSE) cost function compared with other cost functions based on smoothed and unsmoothed datasets to obtain the best model. Section V illustrates the performance of the DRM for the dynamic adjustment of operational parameters to regulate the earth pressure for a real tunneling case in Luoyang, China.

II. METHODOLOGY

A. GRU-BASED DRM FRAMEWORK

To realize the automatic regulation of earth pressure, the GRU-based DRM framework consisted of three main sections: data pre-processing, the GRU model for earth pressure prediction, and the DRM for earth pressure regulation as shown in Fig 1.

During EPB shield tunneling, excavated materials in the soil chamber are plasticized with additives such as foam and slurry and then used to maintain the stability of the excavation face. The process of balancing the earth pressure at the excavation face by adjusting the input and output of excavated materials is known as earth pressure regulation. Generally, the earth pressure monitored at a bulkhead is approximated as the earth pressure of the excavation face and is a significant assumption for earth pressure regulation. The monitored earth pressure is closely associated with the shield operational parameters including the advance rate and screw conveyor speed. Therefore, operational parameters recorded by the data acquisition system of the EPB shield machine combined with the geometric and geological parameters of the tunnel establish the database in real time as shown in Fig. 1.

The GRU model was developed using a continuously updated database to reflect the non-linear mapping between the operational parameters and the earth pressure. The GRU model was improved by a new proposed cost function (REMSE) and a data smoothing technique called moving average smoothing (MAS) was used in this research to obtain the best prediction model (Model A in Fig. 1).

The DRM of operational parameters were built based on the prediction model. By combining the historical database, the current geological and geometric information, and the preset operational parameters, Model A predicts the earth pressure of the next segment. If the earth pressure is beyond the suggested range, the preset operational parameters are optimized by the GA-based optimizer in the DRM. The optimized preset operational parameters are then recommended for the construction of the next segment, and the construction database is updated with the monitored data of the next segment. This process continues until all the segments have been completed, thus realizing construction automation and intelligence.

B. GRU METHOD

1) GRU RECURRENT NEURAL NETWORKS

GRU neural networks are composed of an input layer, hidden layers, and an output layer [49] as illustrated in Fig. 2. In the input layer, the sequential input data are labelled as $X = (x_1, x_2, \ldots, x_t)$, where $x_t \in \mathrm{R}^n$ refers to the input feature vector at the t-th time step. The input data pass into the recurrent hidden layers via the weighted connections.

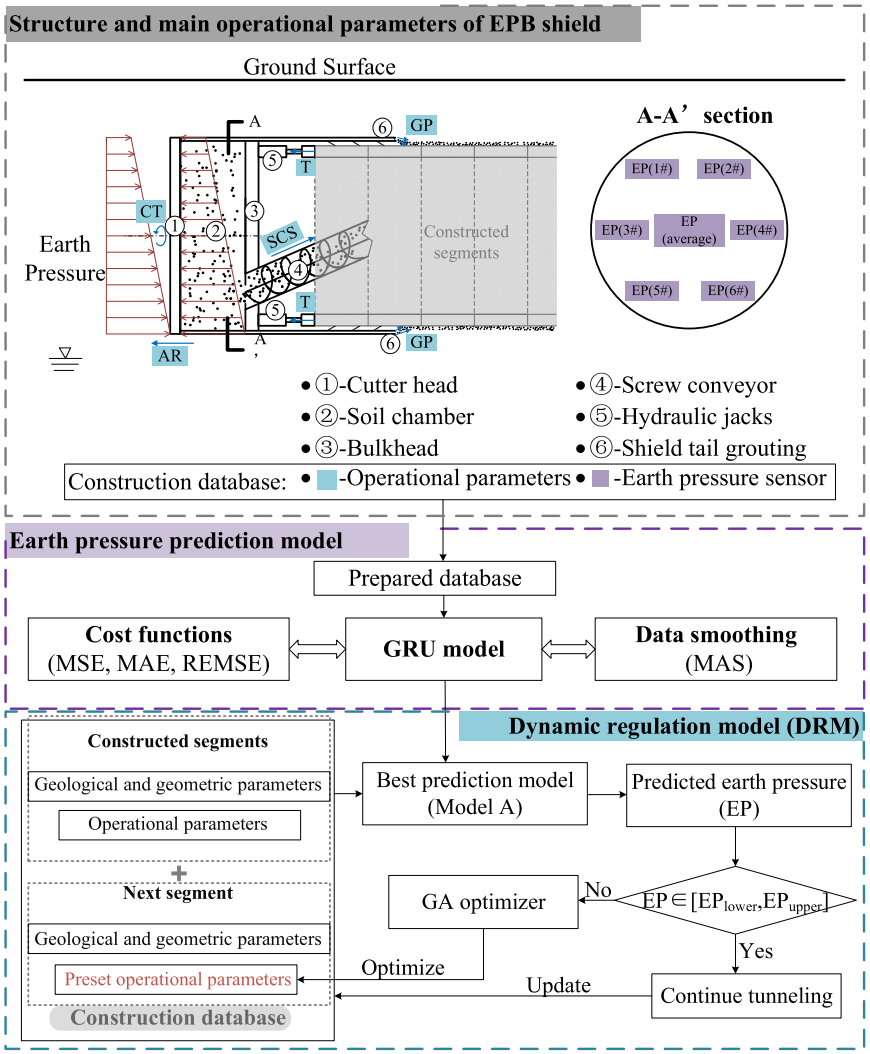

FIGURE 1. Frame of earth pressure prediction and regulation during tunneling.

The recurrent hidden output state at the t-th time step (h_t in Fig. 2) is operated on by the GRUs and updated over time. The input of the GRUs contains not only the input at the current time step (t) but also the hidden state at the previous time step (t - 1). The output of the GRUs then passes to the fully connected hidden units or to the output layer directly. The GRU neural network used in this study was the many-to-one type.

GRUs import two gate operations: the reset gate (r_t) and the update gate (u_t). The reset gate squashes the hidden state at the previous time step to the range [0, 1] to consider the influence of the historical data. More historical information will be ignored when the value approaches 1. The update gate represents the significance of the current information. The value of the update gate is also scaled to [0, 1]; the greater the value, the greater the value of output resources from the current input and the data from the previous hidden state is forgotten. The calculations for the GRU neural network are:

$$\begin{aligned} r_t &= \sigma(W_r \cdot [x_t, h_{t-1}] + b_r) \\ u_t &= \sigma(W_u \cdot [x_t, h_{t-1}] + b_u) \\ \tilde{h}_t &= \tanh(W_h \cdot [x_t, r_t \odot h_{t-1}] + b_h) \\ h_t &= (1 - u_t) \odot h_{t-1} + u_t \odot \tilde{h}_t \\ \sigma(x) &= \frac{1}{1 + e^{-x}} \\ \tanh(x) &= \frac{e^x - e^{-x}}{e^x + e^{-x}}, \end{aligned} \tag{1}$$

where, subscript t denotes the time step, W_r, W_u, W_h represents the weights matrixes of the reset gate, the update gate, the hidden state in the GRU units, respectively, b_r, b_u, b_h gate, and the hidden state in the GRUs, respectively; $\tilde{h}_t$ represents the calculated element of the hidden state (h_t); and the symbol $\odot$ denotes the Hadamard product (element-wise multiplication).

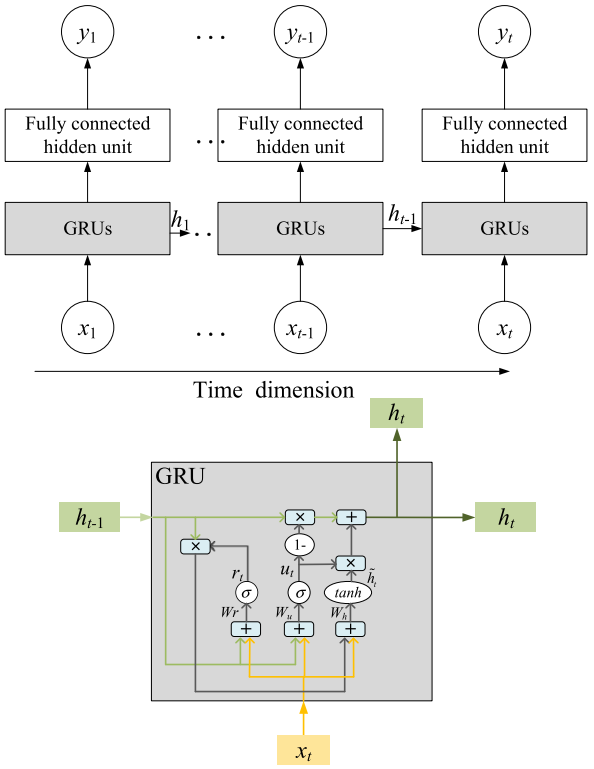

FIGURE 2. Data flow diagram for GRU neural networks (created based on the concept from [49]).

2) COST FUNCTIONS

A training process of the neural network was performed to minimize the error between the output and the target value. Therefore, the error described by the cost function greatly affects the performance of the trained model. Most GRU neural networks are conventionally integrated with mean square error (MSE) or mean absolute error (MAE) cost functions in the regression tasks to assess the absolute error definition. However, conventional cost functions ignore the magnitude diversity of samples, where small-value samples contribute less to the gradient of weights than do large-value samples. The diversity induces an uneven gradient descent for different samples and lowers the convergence rate in the backpropagation process. Therefore, a new relative error-based cost function, the REMSE, was proposed to enlarge the errors of the small-value samples and thus average the gradient of the different samples and accelerate the training process [50]. The vanishing gradient problem was also eliminated because of the enlarged errors in the backpropagation.

The definitions of the MSE, MAE, and REMSE cost functions are given as:

$$J_0^{MSE} = \frac{1}{N}\sum_{i}^{N}(y_{oi} - y_i)^2$$

$$J_0^{MAE} = \frac{1}{N}\sum_{i}^{N}|y_{oi} - y_i|$$

$$J_0^{REMSE} = \frac{1}{N}\sum_{i}^{N}\left(\frac{y_{oi} - y_i}{y_i}\right)^2$$

$$J^* = J_0^* + \lambda\sum_{j} w_j^2 \tag{2}$$

where J_0^{MSE}, J_0^{MAE}, and J_0^{REMSE} represent the MSE, MAE, and REMSE cost functions, respectively; J^* represents the corresponding cost function; N denotes the number of samples in the training set; y_{oi} refers to the predicted output of the i-th sample of the model; y_i refers to the target value of the i-th sample; λ denotes the L2 regularisation coefficient to penalise large weights and reduce overfitting; and w_j denotes the j-th weight in the weight space. A substitute value of 1 is recommended when $y_i = 0$ as the denominator in the REMSE cost function.

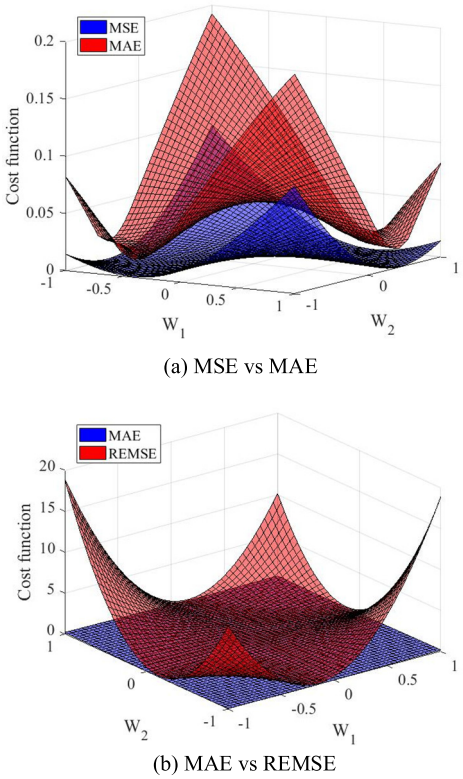

(a) MSE vs MAE

(b) MAE vs REMSE

FIGURE 3. Comparison of MSE, MAE and REMSE cost functions in weight space (a) MSE vs MAE and (b) MAE vs REMSE.

A series of data pairs were picked to visualise the MSE, MAE, and REMSE cost functions in the weight space using a three-layer neural network with one node at each layer as shown in Fig. 3. The input data were $X = [0.1, 0.2, 0.3, 0.4, 0.5]$, and the target data were $y = X^2$. The results confirm the similarity between the MSE and MAE cost functions not only in the slope rate of the surface but also in the value of the cost function. In contrast, the REMSE cost function presented fewer plateaus and a higher slope rate than that of the MSE and MAE cost functions and contributed to a fast gradient descent and convergence in the backpropagation.

In this research, the REMSE cost function was integrated into the GRU neural network for the first time.

C. GA METHOD

The major DRM function of adjusting the predicted earth pressure to the desired value was equivalent to searching for the appropriate input of Model A to optimize the output to the required range. In this research, the GA [51] inspired by the biological evolution of natural selection and genetic mechanism of Darwin's theory was implemented to optimize the input operational parameters. Conventional optimization algorithms based on gradient descent are inappropriate in this system because of the complicated gradient of the output with respect to the input of the GRU model. Unlike conventional optimization algorithms such as the calculus-based and grid search methods, the GA is a type of evolutional optimization method that does not require a continuous or differentiable objective function.

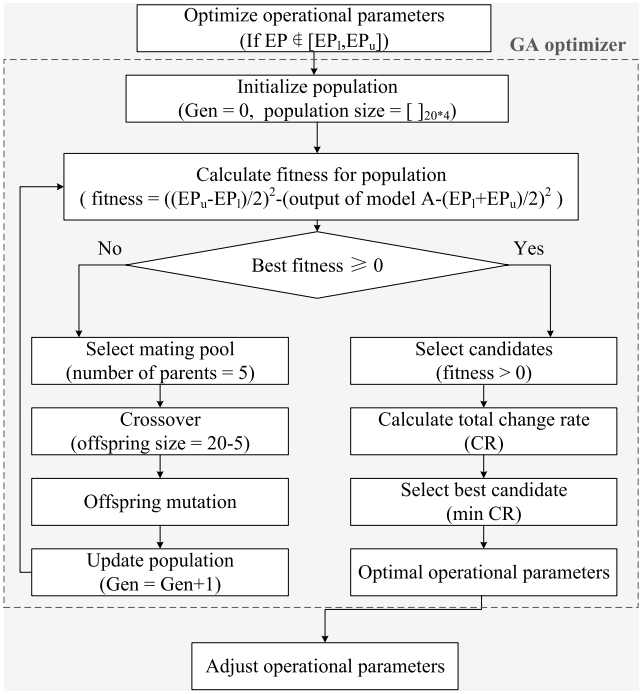

FIGURE 4. GA optimizer flowchart of operational parameter regulation during tunneling.

Fig. 4 shows the flowchart of the GA optimizer in the DRM. When the predicted earth pressure (EP) from Model A is beyond the suggested range [EP$_l$, EP$_u$], the GA optimizer is called to optimize the preset operational parameters. Specific operational parameters selected by a correlation analysis (see Section III D) are optimized to adjust the earth pressure instead of tuning all the input parameters. The GA optimizer is used to generate a population by adding a small random amount to the original preset parameters, and then the fitness is calculated for each one. A better fitness indicates an adjusted earth pressure closer to the midpoint between the lower and upper limits. Then, those candidates with the top fitness are selected to produce a new generation, and simultaneously the offspring go through the process of crossover and mutation. Iteration continues until some candidates meet the earth pressure requirement. Finally, the optimized parameters are selected from the candidates with the lowest change rate compared to the original preset value because a large-scale parameter adjustment during construction is usually not desirable.

III. DATA PREPROCESSING AND MODELLING

A. DATA SOURCE

The GRU-based DRM was verified by an EPB tunneling case of the Luoyang Metro Line 2 located in Henan Province, China. The tunnel section from Luoyang Railway Station to Airport Road Station was investigated in this study (Fig. 5 (a, b)). The size of the EPB shield machine was 6.44 m in diameter and 9.00 m in length with a cutter head opening ratio of approximately 50%. The construction included two parallel lines: the west line with a length of 1173.21 m and the east line with a length of 1172.00 m. The width of each segment was 1.50 m, and each line was composed of approximately 780 segments. The outer diameter and inner diameter of a segment were 6.20 m and 5.50 m, respectively.

The effect of groundwater was ignored because the groundwater table (19.47–21.05 m below ground surface) was below the tunnel structure (maximum cover depth of 14.20 m). The strata in this section was divided into eight classes (Fig. 5 (b)). A few underground caves were discovered in the loess strata. The depths of the cave bottoms ranged from 3.80 m to 10.00 m, and the cave height was generally between 0.80 m and 1.50 m. The tunnel passed mainly through a silty clay stratum.

B. DATA PREPARATION

In the case of earth pressure regulation, the database of the GRU model consisted of the geometry of the tunnel and the geological conditions and tunneling operational parameters. Raw training data and test data were collected every minute from the construction of the east line (765 constructed segments) and west line (773 constructed segments).

Geometric parameters include the shape, size, and cover depth of the tunnel segments. Only the cover depth (CD) of the tunnel was considered as the geometric parameter because the shape and diameter remained unchanged for each segment. CD is defined as the distance from the ground surface to the top of a segment extracted from the geological profile. Generally, it has a positive correlation with earth pressure according to the soil mechanism.

Geological parameters refer to the stratum parameter and include the geometric and mechanical parameters.

Earth pressure is related to the physical and mechanical parameters such as the thickness, cohesion, and internal friction angle of each stratum. For one particular soil stratum, only the thickness varied with the tunnel, whereas the other physical and mechanical parameters remained the same.

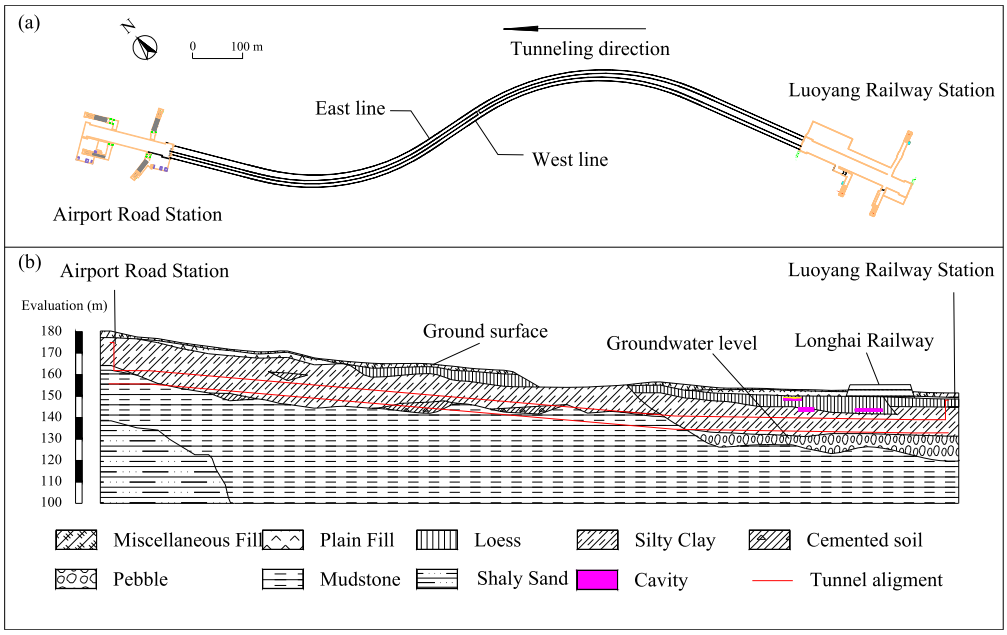

FIGURE 5. Site review: (a) plan view of tunnel section and (b) geological profile of site.

Therefore, only the thickness of each stratum was considered. The excavation process of the EPB shield caused a continuous disturbance to the surrounding soil and changed the soil stress distribution in certain areas. A depth of 40 m (about six times the diameter of the tunnel segment) of strata was considered to be a disturbed area to eliminate the boundary effect.

Real-time operational parameters are usually regulated manually by experienced engineers and can be directly collected through the acquisition system. Operational parameters include: 1) physical parameters: cutter head speed (CS), advance rate (AR), and penetration rate (PR) and speed of the screw conveyor (SCS), 2) mechanical parameters: cutterhead torque (CT) and thrust (T) and grouting pressure (GP), and 3) soil modification materials in the chamber: bentonite volume (BV), foam liquid volume (FLV), and foam air volume (FAV). Physical parameters such as CS, AR, and PR determine the speed of soil excavation. A higher excavation speed means more soil into the chamber, causing a higher monitored earth pressure. In contrast, SCS determines the speed of soil discharge. A higher discharge speed results in more soil being transported out of the chamber and reduces the monitored earth pressure. Mechanical parameters reflect the interaction between the cutting face and the surrounding strata. The magnitude of these parameters also has a direct impact on the soil stress state.

Before the raw data were imported into the GRU model, data pre-processing was performed and involved the following steps.

1) STEP 1: REMOVAL OF EMPTY PUSH DATA

Raw data include both working-state data and empty push-state data. Empty push data account for a large proportion of the dataset. The first step is to remove the empty push data according to

$$Q = f(\mathrm{CS}) \cdot f(\mathrm{AR}) \cdot f(\mathrm{PR}) \cdot f(\mathrm{CT}) \cdot f(\mathrm{T})$$
$$f(x) = \begin{cases} 0, & x = 0 \\ 1, & x \neq 0 \end{cases}, \tag{3}$$

where $f(x)$ is a function to seek the 0 element in variables (CS, AR, PR, CT, and T), and Q is a product operation of multiple $f(x)$. When $Q = 0$, at least one of the variables equals 0 and can be removed as empty push data.

2) STEP 2 EXCLUSION OF OUTLIER DATA

For each segment, outlier data which deviate more than three times the standard deviation away from the average value are eliminated according to the Pauta criterion [52].

3) STEP 3 UNIFICATION OF DATASET SIZE

Limited by the acquisition of real-time geological parameters, the geological parameters in the input data are only extracted from the geological profile for each segment. The data recorded by the tunneling system are converted to the average value for each segment.

4) STEP 4 NORMALISATION

To improve the training process, the dataset is normalized to the interval (0,1) by dividing 1.2 times of the maximum value, which could retain the original characteristics of the raw dataset and also achieves a faster convergence.

The training dataset contained 763 samples from the east line, and the test dataset included 771 samples from the west line.

C. DATA SMOOTHING (MAS METHOD)

In the soil excavation of EPB tunneling, the cutter head continually rotates to cut out the soil. The excavated soil rolls into the chamber in a non-static equilibrium state. The monitored earth pressure is not equivalent to the real earth pressure because of the disturbed state. Therefore, the deviation between the monitored and real earth pressure adds noise to the datasets, slows down the training process, and reduces the accuracy of the GRU model. To eliminate the effect of noise and improve the performance of the GRU model, MAS was implemented. Two types of datasets (smoothed and unsmoothed) were prepared to investigate the influence of data smoothing on the prediction accuracy of the trained model (Section IV B). The moving window width of MAS is defined as 3 because the range of influence of the disturbed earth pressure has been proven to be limited to three segments. The smoothed data $\overline{x_t}$ at time step t equals the average of the data at time steps t - 2, t – 1, and t. The MAS method effectively reduced the noise of the dataset, and the standard deviation (STD) decreased as shown in Table 1.

TABLE 1. Statistics of input and output variables of GRU model.

Parameters (Unit)	Type	Statistics (smoothed / unsmoothed)				GRG
		Min	Max	Aveg	STD	
SCS (rpm)	I	4.76 2.28	12.57 13.00	8.51 8.50	1.63 1.79	0.735
CS (rpm)	I	1.23 1.06	1.97 2.02	1.67 1.67	0.13 0.15	0.728
CT (kN·m)	I	1068.49 989.16	3805.87 4036.85	2197.52 2197.41	559.33 580.60	0.725
AR (mm/min)	I	32.55 17.00	88.25 91.93	64.80 64.72	10.34 12.07	0.704
BV (m^3)	I	58.70 26.35	996.11 1008.59	517.26 516.72	184.48 195.64	0.700
FAV (m^3)	I	102.72 82.76	1045.77 1097.56	556.42 556.69	153.89 171.78	0.685
PR (mm/r)	I	20.46 13.87	52.72 55.33	38.84 38.81	5.14 6.40	0.680
FLV (m^3)	I	56.65 23.93	132.11 136.25	79.36 79.40	6.88 8.85	0.679
T (kN)	I	5676.03 5212.38	12372.05 13368.18	9222.67 9213.86	1166.87 1342.31	0.670
GP (kPa)	I	12.63 0	330.83 397.92	101.61 101.53	36.25 42.20	0.658
CD (m)	I	8.10 8.10	16.33 16.33	13.41 13.41	1.69 1.68	0.651
Thickness of each stratum (m)	I	…	…	…	…	…
Eearth Pressure (kPa)	I /O	56.19 29.69	205.14 210.44	163.71 163.42	16.18 18.73	

*Note: I refers to input and O refers to output.

D. GREY RELATIONAL ANALYSIS

Grey relational analysis (GRA) proposed by Deng [53] has been useful in determining the complicated interrelationship between multiple variables. In this research, GRA was used to measure the correlation or grey relational grade (GRG) between the output (earth pressure) and the input variables (operational parameters) of the GRU model according to their development trend over time. The most relevant parameters were determined to guide the earth pressure regulation by the DRM. Data were first normalized to avoid different units and reduce the variability. The normalisation formula is

$$\tilde{x}_i(k) = \frac{\max(x_i) - x_i(k)}{\max(x_i) - \min(x_i)}, \tag{4}$$

where $\tilde{x}_i(k)$ is the normalized value of the i-th input variable at the k-th segment, $x_i(k)$ is the original value of the i-th input variable at the k-th segment, and $k = 1, 2, \ldots, N$ is the number of segments.

The next step is to calculate the absolute deviation Δ_{oi} of the input variable x_i and the output variable x_o and determine the maximum and minimum values of Δ_{oi} Then, the grey relational coefficient $\xi_i\,(k)$ is calculated as

$$\xi_i(k) = \frac{\Delta_{\min} + \xi\,\Delta_{\max}}{\Delta_{oi}(\mathrm{k}) + \xi\,\Delta_{\max}}$$
$$where,\ \Delta_{oi}(k) = |x_o(k) - x_i(k)|\,,\ \xi = 0.5, \tag{5}$$

The final step is to calculate the GRG. The GRG denoted by γ_i, represents the level of correlation between the output variable x_o and the input variable x_i. The formula is

$$\gamma_i = \frac{1}{m}\sum_{k=1}^{m}\xi_i(k), \tag{6}$$

The results of GRA and other statistics of the input and output variables of the smoothed and unsmoothed training set are shown in Table 1. The thickness of each stratum was omitted in Table 1.

E. GRU MODELLING

Fig. 6 shows the four-layer architecture of the network consisting of one input layer, one GRU layer, one fully connected layer, and one output layer. The input layer contained 22 nodes consisting of 10 operational parameters, 1 geometric parameter, 10 geological parameters, and the earth pressure measurement of the previous segment. The number of nodes in the hidden layers was determined by the trial and error method. Twenty nodes in each layer were observed to obtain the minimum MSE. The output layer had only one node for earth pressure. The momentum stochastic gradient descent algorithm was adopted with the hyper-parameter $\alpha = 0.9$ to accelerate convergence. In addition, the particle swarm optimization method was implemented to optimize the initial learning rate to 0.01877, multiplying a scaling index of 0.5 after each 2,000 epochs. Here, multiple trials have found that an L2 regularisation of 0.001 is the most conducive to model training. The number of training epochs was set to 8,000, after which no significant decrease in MSE or REMSE was observed. The time step was set to 5 [48] to contain the input variables of the current and the previous four segments. The random normal initialisation method and a batch size of 100 were adopted according to the results of trial and error. Each experiment was repeated three times, and the results are the average of the three experiments for each model.

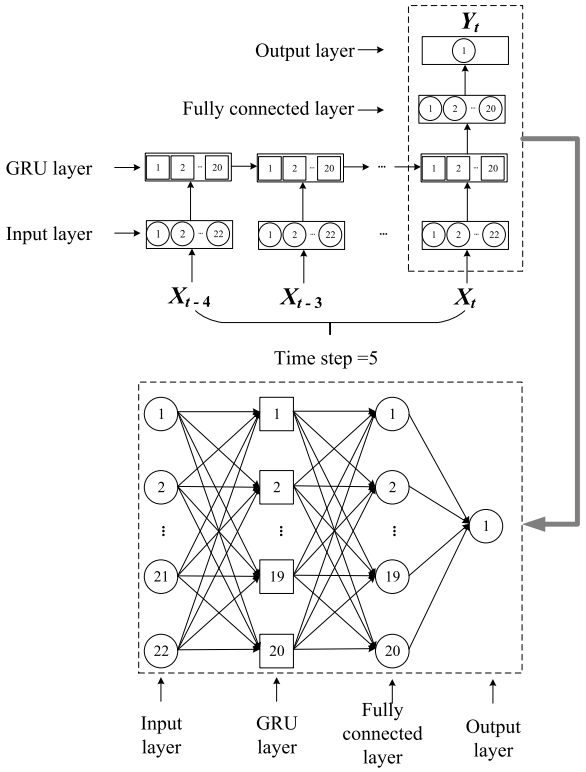

FIGURE 6. Architecture of GRU model for earth pressure prediction (recreated on the concept of [48]).

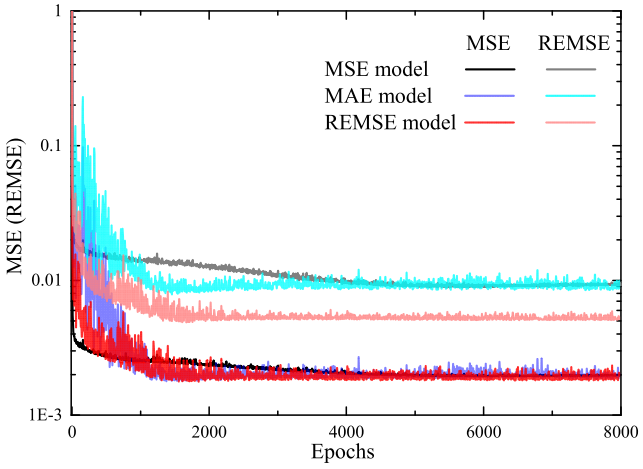

FIGURE 7. Performance comparison of GRU model using different cost functions.

IV. GRU MODEL RESULTS AND DISCUSSION

A. IMPROVEMENT BY REMSE COST FUNCTION

Fig. 7 shows the MSE and REMSE values between the target (y_i) and the output (y_{oi}) of the GRU models with different cost functions (namely, MSE model, REMSE model and MAE model) during the training process. As Fig. 7 illustrates, regardless the cost function used, the converged MSE was lower than the REMSE. This is easily proved by the definition of MSE and REMSE given in (2). MSE denotes the absolute error, whereas REMSE denotes the relative error. When y_{oi} approaches y_i, the absolute difference becomes much smaller than the relative difference.

From the perspective of convergence rate, the REMSE model had a more rapid decline in both MSE and REMSE than that of the MAE and MSE models. From the perspective of convergence, the MSE model had the largest error assessed by MSE or REMSE. In contrast, the REMSE model outperformed the other models both in the final convergence value and the stability of convergence. Both the converged MSE and REMSE values of the REMSE model in the training dataset were lower than that of the MAE model, and the REMSE model exhibited the least fluctuation during the convergence process. The MSE values of the different models were similar for both the training and test datasets as shown in Table 2. However, the REMSE model obtained the smallest REMSE value in the training and test datasets, which confirms the effectiveness of the REMSE cost function. To conclude, the REMSE model outperformed the other models in convergence speed, error value, and stability calculation. Therefore, the REMSE cost function was utilized as the cost function for the best model.

TABLE 2. MSE and REMSE error of different GRU models.

GRU networks	MSE value		REMSE value	
	Training (10^{-3})	Test (10^{-3})	Training (10^{-3})	Test (10^{-2})
MSE model	2.02	8.41	9.83	4.32
MAE model	1.96	6.89	9.10	3.47
REMSE model	1.91	7.03	5.19	3.31

B. IMPROVEMENT BY MAS METHOD

The unsmoothed dataset was first used to train and test the GRU model. Results reveal that the average absolute relative error of prediction of the unsmoothed training dataset was 5.35% and that of the unsmoothed test dataset was 10.64%. Even though the predicted earth pressure presented a trend consistent with that of the target value, a large deviation between the predicted and target values still existed. With repeated experiments and particle swarm optimization, we are confident that the deviation was associated with dataset noise. The earth pressure was monitored by the stress gauges installed on the bulkhead. Monitored earth pressure is usually considered to be equivalent to the real earth pressure based on static equilibrium. In fact, the soil in a chamber is always in a disturbed state because of the rotation of the cutter head and the simultaneous mixture with various additives. The disturbance breaks the static equilibrium and introduces excessive noise to the monitored earth pressure. The noise creates poor dataset quality and accounts for the poor performance of the trained model.

To eliminate the noise and improve the prediction accuracy, the MAS method was implemented to smooth the datasets before training (Section III C). Fig. 8 shows the prediction

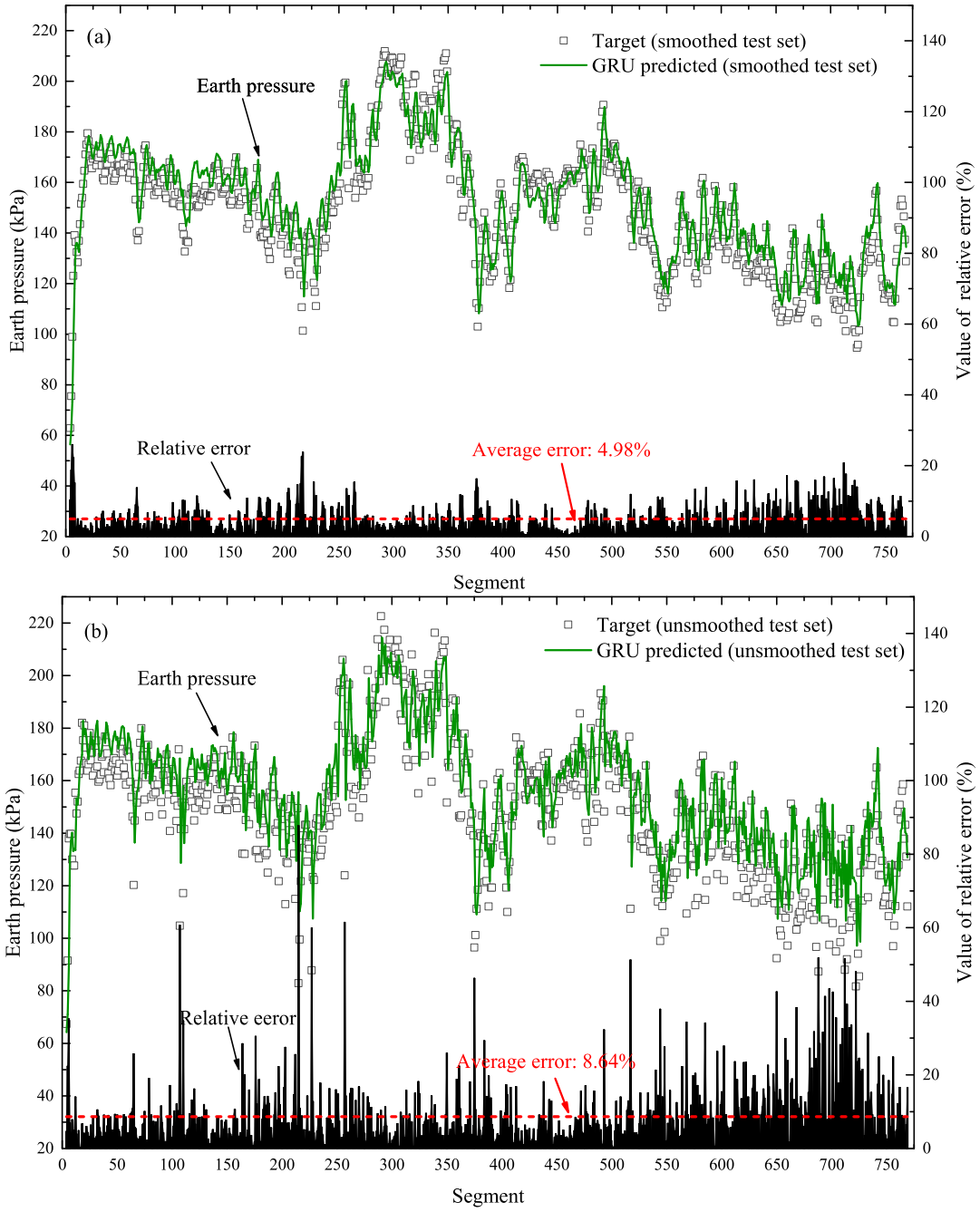

FIGURE 8. Results of GRU model trained by smoothed training set using (a) smoothed test set and (b) unsmoothed test set.

of smoothed and unsmoothed test datasets of the GRU model with MAS. The average absolute relative error of the smoothed test set was 4.98%, and when the original unsmoothed test set was imported to the GRU model, the average absolute relative error of the unsmoothed test set was reduced from 10.64% to 8.64%.

To examine the correlation of the predicted and the monitored earth pressure, the coefficient of determination (R^2) was used. For a good regression model, the value of R^2 is between 0 and 1, and the closer it is to 1, the better the model. The formula is

$$R^2 = 1 - \frac{\sum_i^m (y_i - y_{oi})^2}{\sum_i^m (y_i - \bar{y})^2}, \tag{7}$$

where, $\bar{y}$ is the average of the actual value.

The correlation between the predicted and monitored earth pressure of GRU models with and without MAS method is shown in Fig. 9. Most of the scattered points in Fig. 9 (a) are deviated from the line $y = x$, which indicates the overall great difference between the predicted value and monitored one. By implementing MSA method, the scattered points in Fig. 9 (b, c) converge towards $y = x$. For the unsmoothed test set, R^2 increases from 0.49 to 0.63. And R^2 for smoothed test is increased to 0.88 significantly.

V. DRM FOR OPERATIONAL PARAMETERS

A. GA STOPPING CRITERIA

The GA stopping criteria should be associated with the regulation standards of earth pressure in the DRM and consider not only the desired earth pressure but also the error from the prediction of the GRU model.

The earth pressure regulation in tunneling construction commonly refers to the limit state control method based on Rankine's earth pressure theory [54]. The earth pressure of soil in the natural state is called static earth pressure (P_0). During tunneling, the rotation and squashing of the cutter head disturbs the static equilibrium state of soil and results in an active ($P_a < P_0$) or passive ($P_p > P_0$) earth pressure. When the earth pressure in a soil chamber decreases and causes the soil in front of the chamber to reach the ultimate equilibrium state, the earth pressure at the excavation face becomes active. On the contrary, when the earth pressure in a soil chamber increases and causes the soil in front of the chamber to reach the ultimate equilibrium state, the earth pressure at the excavation face becomes passive. The calculations for earth pressure in different states are

$$\begin{aligned} P_0 &= K_0\sigma_z = K_0\gamma z \\ P_a &= \sigma_z \tan^2(45^\circ - \frac{\varphi}{2}) - 2c\tan(45^\circ - \frac{\varphi}{2}) \\ P_p &= \sigma_z \tan^2(45^\circ - \frac{\varphi}{2}) + 2c\tan(45^\circ - \frac{\varphi}{2}), \end{aligned} \tag{8}$$

where K_0 is the coefficient of lateral pressure, σ_z is the vertical stress at depth z, γ is the unit weight of the soil, C is the cohesion of the soil, and φ is the internal friction angle.

In tunneling construction, the earth pressure is expected to be set within a range $[P_a, P_p]$ as small as possible to reduce cutter wear and energy consumption. Zizka and Thewes [55] suggested that the earth pressure should be set near the static earth pressure with a maximum deviation of 30 kPa. Considering the prediction error of the GRU model, the median relative error of -3.50% of the predicted earth pressure compensates for the output of the GRU model in the DRM. The following formulas give the adjusted upper and lower bounds considering the median

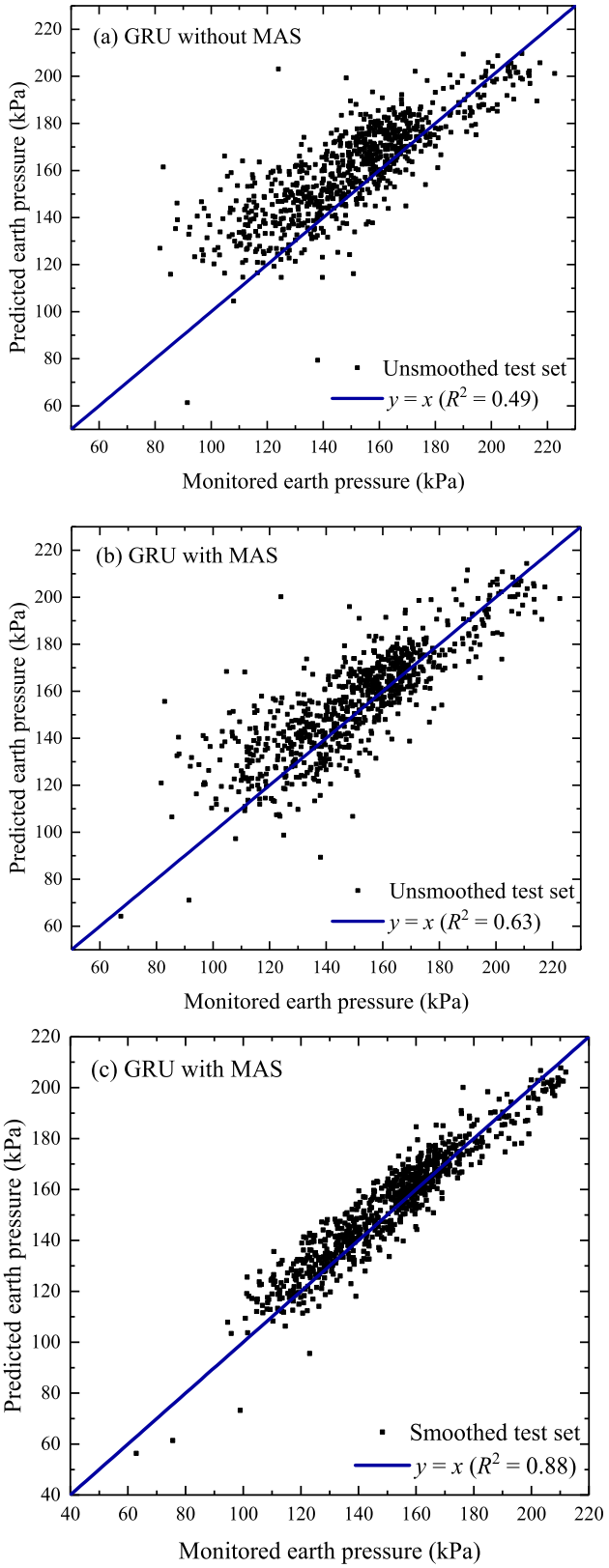

FIGURE 9. Correlation of predicted and monitored earth pressure for models: (a) GRU without MAS (unsmoothed test set), (b) GRU with MAS (unsmoothed test set), and (c) GRU with MAS (smoothed test set).

relative error:

$$\begin{aligned} |P_{0i} - y_i| &\leq 30kPa \\ e &= \frac{y_{oi} - y_i}{y_i} \\ &\Rightarrow y_i = \frac{y_{oi}}{1+e} \\ &\Rightarrow (1+\mathrm{e})(P_{0i} - 30) \leq y_{oi} \leq (1+\mathrm{e})(P_{0i} + 30), \end{aligned} \tag{9}$$

where P_{0i} is the static earth pressure for the i-th segment, y_i and y_{oi} are the actual monitored earth pressure and output of model A for the i-th segment, respectively, and e is the median prediction error rate.

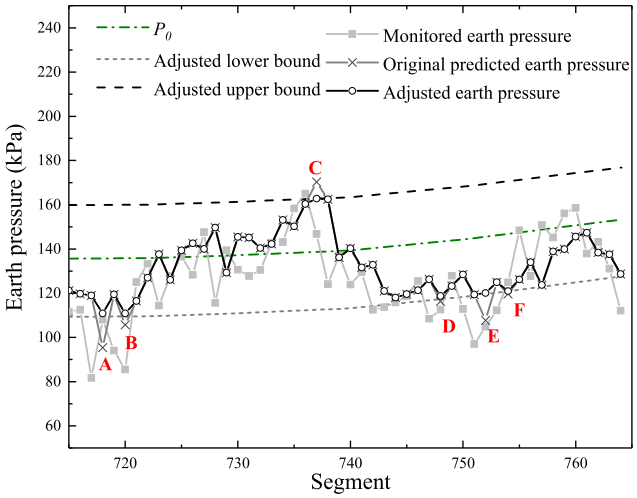

FIGURE 10. Results of earth pressure regulation by DRM for operational parameters.

B. DRM PERFORMANCE

The last 50 segments were used to verify the effectiveness of the DRM for operational parameter adjustments. According to the results of the GRA in Section III D, four parameters—SCS, CS, CT, and AR—were selected as the adjusted parameters because of their higher correlations with earth pressure. Fig. 10 shows the regulated earth pressure of the DRM. The predicted earth pressures of the GRU model for segments A–F exceeded the control range; therefore operational parameter regulation was required. By applying the DRM for operational parameters, the predicted earth pressures of segments A–F were successfully adjusted to the allowed range. In addition, the actual monitored earth pressure at segments A, B, D, and E exceeded the control range. This means that four out of six adjusted segments were successfully predicted to exceed the limit and were effectively regulated. However, the regulation of earth pressure relies heavily on the accuracy of the prediction model. Some segments exceeded the control range but were not predicted and correctly regulated.

Fig. 11 shows the corresponding adjustment of operational parameters for each segment by the DRM. In general, the magnitude of rate change of each parameter was

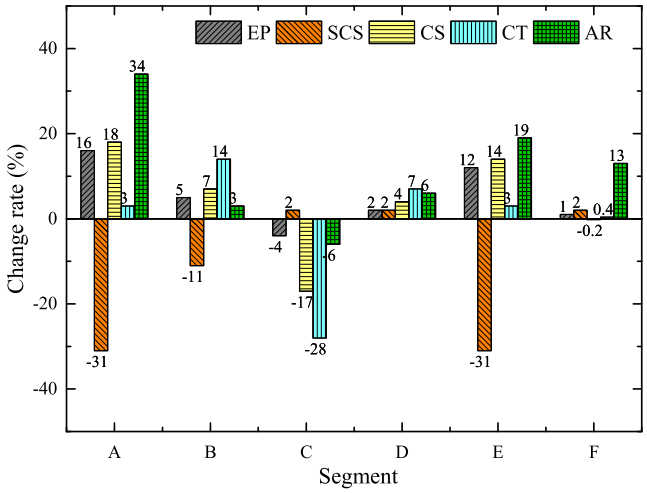

FIGURE 11. Adjustment of specific operational parameters for segments A-F by DRM during tunneling.

less than 34%, which satisfies the goal of avoiding abrupt parameter adjustments. Some patterns can also be observed from the adjustment of different segments. For example, the adjustment of the parameters for segments A and E had the same pattern because the geological conditions of A and E were similar. To increase the earth pressure by more than 10%, the speed of the screw conveyer must decrease by more than 30%. As a result, less soil is transported out of the soil chamber, and the cutter-head speed, torque, and advance rate all increase by different amounts. These three parameters (CS, CT, and AR) are closely related to the excavation of soil, and a positive increase also means an increase in the amount of soil in the chamber. Meanwhile, the more the earth pressure is increased, the greater the magnitude of the adjustment of these four parameters. For segment C, the earth pressure was reduced by increasing SCS and decreasing CS, CT, and AR, which is the opposite of the adjustment for segments A and E.

The above results show the feasibility of the DRM for the adjustment of operational parameters to dynamically regulate earth pressure in real-time. This method gives an operator practical operational guidance as the adjustment of the parameters is quantified.

VI. CONCLUSION

This study proposed an intelligent framework to predict and then automatically regulate earth pressure using the deep learning technique incorporated with a GA during EPB shield tunneling. The proposed models were applied to a metro tunnel construction field case in Luoyang, China. The following conclusions were drawn.

(1) The proposed framework integrated an REMSE cost function with a GRU deep learning technique. Compared to the GRU models based on MSE and MAE cost functions, the REMSE cost function provides the best convergence rate, stabilisation calculation, and

error value. In a GRU, the MAS method reduces the noise and improves the dataset quality. The smoothed dataset improved the model performance with R^2 increasing by 50% and the average relative error decreasing by 20%.

(2) Based on the GRU results, the proposed DRM for earth pressure control regulated the predicted earth pressure by adjusting the operational parameters. In the DRM, the suggested earth pressure range was first calculated using Rankine's earth pressure theory with consideration of the model prediction error. Then, a GA optimizer was adopted to search for the optimal operational parameters to output the expected earth pressure with the least adjustment.

(3) The field observed data from metro tunnel construction in Luoyang were used to verify the proposed models. The results showed that the proposed GRU model with MAS can predict the earth pressure reasonably well with the lowest relative error of 4.98% on the smoothed test set and 8.64% on the unsmoothed test set. The DRM using GA optimizer automatically regulate the earth pressure predicted by GRU model to the suggested range through adjusting four key operation parameters. The adjustment result is in accordance with the construction experiences, which confirms the effectiveness of the proposed model.

ACKNOWLEDGMENT

The author sincerely appreciate the support from the Luoyang Metro Line 2 Project Department of China Railway 16th Bureau Group, Jiaxuan Zhang and Kun Zhang for the collection of the field data in this work.

REFERENCES

[1] D.-J. Ren, J. S. Shen, J.-C. Chai, and A. Zhou, "Analysis of disc cutter failure in shield tunnelling using 3D circular cutting theory," *Eng. Failure Anal.*, vol. 90, pp. 23–35, Aug. 2018, doi: 10.1016/j.engfailanal.2018.02.015.

[2] D.-J. Ren, S.-L. Shen, A. Arulrajah, and W.-C. Cheng, "Prediction model of TBM disc cutter wear during tunnelling in heterogeneous ground," *Rock Mech. Rock Eng.*, vol. 51, no. 11, pp. 3599–3611, Nov. 2018, doi: 10.1007/s00603-018-1549-3.

[3] D.-J. Ren, S.-L. Shen, A. Arulrajah, and H.-N. Wu, "Evaluation of ground loss ratio with moving trajectories induced in double-O-tube (DOT) tunnelling," *Can. Geotech. J.*, vol. 55, no. 6, pp. 894–902, Jun. 2018, doi: 10.1139/cgj-2017-0355.

[4] Y.-X. Wu, S.-L. Shen, H.-M. Lyu, and A. Zhou, "Analyses of leakage effect of waterproof curtain during excavation dewatering," *J. Hydrol.*, vol. 583, Apr. 2020, Art. no. 124582, doi: 10.1016/j.jhydrol.2020.124582.

[5] Q.-L. Cui, H.-N. Wu, S.-L. Shen, Y.-S. Xu, and G.-L. Ye, "Chinese karst geology and measures to prevent geohazards during shield tunnelling in karst region with caves," *Natural Hazards*, vol. 77, no. 1, pp. 129–152, May 2015, doi: 10.1007/s11069-014-1585-6.

[6] H.-N. Wu, S.-L. Shen, S.-M. Liao, and Z.-Y. Yin, "Longitudinal structural modelling of shield tunnels considering shearing dislocation between segmental rings," *Tunnelling Underground Space Technol.*, vol. 50, pp. 317–323, Aug. 2015, doi: 10.1016/j.tust.2015.08.001.

[7] H. N. Wu, S. L. Shen, and J. Yang, "Identification of tunnel settlement caused by land subsidence in soft deposit of Shanghai," *J. Perform. Constructed Facilities*, vol. 31, no. 6, 2017, Art. no. 04017092, doi: 10.1061/(asce)cf.1943-5509.0001082.

[8] H.-N. Wu, S.-L. Shen, J. Yang, and A. Zhou, "Soil-tunnel interaction modelling for shield tunnels considering shearing dislocation in longitudinal joints," *Tunnelling Underground Space Technol.*, vol. 78, pp. 168–177, Aug. 2018, doi: 10.1016/j.tust.2018.04.009.

[9] N. Zhang, J. S. Shen, A. Zhou, and A. Arulrajah, "Tunneling induced geohazards in mylonitic rock faults with rich groundwater: A case study in guangzhou," *Tunnelling Underground Space Technol.*, vol. 74, pp. 262–272, Apr. 2018, doi: 10.1016/j.tust.2017.12.021.

[10] H.-M. Lyu, S.-L. Shen, A. Zhou, and J. Yang, "Perspectives for flood risk assessment and management for mega-city metro system," *Tunnelling Underground Space Technol.*, vol. 84, pp. 31–44, Feb. 2019, doi: 10.1016/j.tust.2018.10.019.

[11] H.-M. Lyu, S.-L. Shen, A. Zhou, and J. Yang, "Risk assessment of mega-city infrastructures related to land subsidence using improved trapezoidal FAHP," *Sci. Total Environ.*, vol. 717, May 2020, Art. no. 135310, doi: 10.1016/j.scitotenv.2019.135310.

[12] H. M. Lyu, S. L. Shen, J. Yang, and A. N. Zhou, "Risk assessment of earthquake-triggered geohazards surrounding Wenchuan, China," *Natural Hazards Rev.*, 2020.

[13] H. M. Lyu, W. J. Sun, S. L. Shen, and A. N. Zhou, "Risk assessment using a new consulting process in fuzzy AHP," *J. Construct. Eng. Manage.*, vol. 146, no. 3, 2020, Art. no. 04019112, doi: 10.1061/(ASCE)CO.1943-7862.0001757.

[14] H.-M. Lyu, J. Shen, and A. Arulrajah, "Assessment of geohazards and preventative countermeasures using AHP incorporated with GIS in Lanzhou, China," *Sustainability*, vol. 10, no. 2, Jan. 2018, Art. no. 304, doi: 10.3390/su10020304.

[15] P. G. Atangana Njock, S.-L. Shen, A. Zhou, and H.-M. Lyu, "Evaluation of soil liquefaction using AI technology incorporating a coupled ENN / t-SNE model," *Soil Dyn. Earthq. Eng.*, vol. 130, Mar. 2020, Art. no. 105988, doi: 10.1016/j.soildyn.2019.105988.

[16] P. G. Atangana Njock, S.-L. Shen, A. Zhou, and H.-M. Lyu, "Data on a coupled ENN / t-SNE model for soil liquefaction evaluation," *Data Brief*, vol. 29, Apr. 2020, Art. no. 105125, doi: 10.1016/j.dib.2020.105125.

[17] G. Anagnostou and K. Kovári, "Face stability conditions with earth-pressure-balanced shields," *Tunnelling Underground Space Technol.*, vol. 11, no. 2, pp. 165–173, 1996, doi: 10.1016/0886-7798(96)00017-X.

[18] M. Chen, S.-L. Shen, A. Arulrajah, H.-N. Wu, D.-W. Hou, and Y.-S. Xu, "Laboratory evaluation on the effectiveness of polypropylene fibers on the strength of fiber-reinforced and cement-stabilized shanghai soft clay," *Geotextiles Geomembranes*, vol. 43, no. 6, pp. 515–523, Nov. 2015, doi: 10.1016/j.geotexmem.2015.05.004.

[19] X.-X. Liu, S.-L. Shen, Y.-S. Xu, and Z.-Y. Yin, "Analytical approach for time-dependent groundwater inflow into shield tunnel face in confined aquifer," *Int. J. Numer. Anal. Methods Geomech.*, vol. 42, no. 4, pp. 655–673, Feb. 2018, doi: 10.1002/nag.2760.

[20] X.-X. Liu, S.-L. Shen, A. Zhou, and Y.-S. Xu, "Evaluation of foam conditioning effect on groundwater inflow at tunnel cutting face," *Int. J. Numer. Anal. Methods Geomech.*, vol. 43, no. 2, pp. 463–481, Jan. 2019, doi: 10.1002/nag.2871.

[21] S.-L. Shen, H.-N. Wu, Y.-J. Cui, and Z.-Y. Yin, "Long-term settlement behaviour of metro tunnels in the soft deposits of shanghai," *Tunnelling Underground Space Technol.*, vol. 40, pp. 309–323, Feb. 2014, doi: 10.1016/j.tust.2013.10.013.

[22] S.-L. Shen, Q.-L. Cui, C.-E. Ho, and Y.-S. Xu, "Ground response to multiple parallel microtunneling operations in cemented silty clay and sand," *J. Geotech. Geoenviron. Eng.*, vol. 142, no. 5, 2016, Art. no. 04016001, doi: 10.1061/(ASCE)GT.1943-5606.0001441.

[23] Z.-Y. Yin, Y.-F. Jin, J. S. Shen, and P.-Y. Hicher, "Optimization techniques for identifying soil parameters in geotechnical engineering: Comparative study and enhancement," *Int. J. Numer. Anal. Methods Geomech.*, vol. 42, no. 1, pp. 70–94, Jan. 2018, doi: 10.1002/nag.2714.

[24] Z.-Y. Yin, Z.-X. Wu, and P.-Y. Hicher, "Modeling monotonic and cyclic behavior of granular materials by exponential constitutive function," *J. Eng. Mech.*, vol. 144, no. 4, 2018, Art. no. 04018014, doi: 10.1061/(ASCE)EM.1943-7889.0001437.

[25] Y. F. Jin and Z. Y. Yin, "An intelligent multi-objective EPR technique with multi-step model selection for correlations of soil properties," *Acta Geotech.*, early access, 2020, doi: 10.1007/s11440-020-00929-5.

[26] H. Yang, H. Shi, G. Gong, and G. Hu, "Earth pressure balance control for EPB shield," *Sci. China E, Technol. Sci.*, vol. 52, no. 10, pp. 2840–2848, Oct. 2009, doi: 10.1007/s11431-009-0245-7.

[27] Z. Shangguan, S. Li, and M. Luan, "Model reference control for bulkhead pressure of EPB shield in tunneling," *J. Converg. Inf. Technol.*, vol. 5, no. 1, pp. 111–115, Feb. 2010, doi: 10.4156/jcit.vol5.issue1.12.
[28] X. Lu, Y. Zhou, M. Huang, and F. Li, "Computation of the minimum limit support pressure for the shield tunnel face stability under seepage condition," *Int. J. Civil Eng.*, vol. 15, no. 6, pp. 849–863, 2017, doi: 10.1007/s40999-016-0116-0.
[29] M. J. Maynar and L. E. Rodríguez, "Discrete numerical model for analysis of earth pressure balance tunnel excavation," *J. Geotech. Geoenviron. Eng.*, vol. 131, no. 10, pp. 1234–1242, 2005, doi: 10.1061/(ASCE)1090-0241(2005)131:10(1234).
[30] T. Qu, S. Wang, J. Fu, Q. Hu, and X. Zhang, "Numerical examination of EPB shield tunneling-induced responses at various discharge ratios," *J. Perform. Constructed Facilities*, vol. 33, no. 3, 2019, Art. no. 04019035, doi: 10.1061/(ASCE)CF.1943-5509.0001300.
[31] H. Kuwahara, M. Harada, Y. Seno, and M. Takeuchi, "Application of fuzzy reasoning to the control of shield tunnelling," *Doboku Gakkai Ronbunshu*, no. 391, pp. 169–178, 1988, doi: 10.2208/jscej.1988.391_169.
[32] R.-P. Chen, P. Zhang, X. Kang, Z.-Q. Zhong, Y. Liu, and H.-N. Wu, "Prediction of maximum surface settlement caused by earth pressure balance (EPB) shield tunneling with ANN methods," *Soils Found.*, vol. 59, no. 2, pp. 284–295, Apr. 2019, doi: 10.1016/j.sandf.2018.11.005.
[33] R. Chen, P. Zhang, H. Wu, Z. Wang, and Z. Zhong, "Prediction of shield tunneling-induced ground settlement using machine learning techniques," *Frontiers Struct. Civil Eng.*, vol. 13, no. 6, pp. 1363–1378, Dec. 2019, doi: 10.1007/s11709-019-0561-3.
[34] P. Zhang, R.-P. Chen, and H.-N. Wu, "Real-time analysis and regulation of EPB shield steering using random forest," *Autom. Construct.*, vol. 106, Oct. 2019, Art. no. 102860, doi: 10.1016/j.autcon.2019.102860.
[35] P. Zhang, Z. Y. Yin, Y. F. Jin, and G. L. Ye, "An AI-based model for describing cyclic characteristics of granular materials," *Int. J. Numer. Anal. Methods Geomech.*, early access, 2020, doi: 10.1002/nag.3063.
[36] P. Zhang, Z.-Y. Yin, Y.-F. Jin, and T. H. T. Chan, "A novel hybrid surrogate intelligent model for creep index prediction based on particle swarm optimization and random forest," *Eng. Geol.*, vol. 265, Feb. 2020, Art. no. 105328.
[37] X. Liu, C. Shao, H. Ma, and R. Liu, "Optimal earth pressure balance control for shield tunneling based on LS-SVM and PSO," *Autom. Construct.*, vol. 20, no. 4, pp. 321–327, Jul. 2011, doi: 10.1016/j.autcon.2010.11.002.
[38] Y. Kuraoka, "Fuzzy automatic control of the direction in the process of tunneling for large slurry shield," *Tunnel Underground*, vol. 1, no. 5, pp. 27–34, 1991.
[39] J.-Y. Dieulot, L. Dubois, and P. Borne, "Composite fuzzy-conventional controls," in *Proc. IEEE Syst. Man Cybern. Conf. (SMC)*, Oct. 1993, pp. 687–695.
[40] X. Li and Z. Chen, "Fuzzy immune control for shield's earth-pressure-balance simulation system," in *Proc. 4th Int. Conf. Natural Comput.*, 2008, pp. 648–652.
[41] I. C. Yeh, "Application of neural networks to automatic soil pressure balance control for shield tunneling," *Automat. Construct.*, vol. 5, no. 5, pp. 421–426, 1997, doi: 10.1016/S0926-5805(96)00165-3.
[42] K. Elbaz, S. L. Shen, A. Zhou, D. J. Yuan, and Y. S. Xu, "Optimization of EPB shield performance with adaptive neuro-fuzzy inference system and genetic algorithm," *Appl. Sci.*, vol. 9, no. 4, p. 780, 2019. [Online]. Available: https://www.mdpi.com/2076-3417/9/4/780
[43] K. Elbaz, S.-L. Shen, W.-J. Sun, Z.-Y. Yin, and A. Zhou, "Prediction model of shield performance during tunneling via incorporating improved particle swarm optimization into ANFIS," *IEEE Access*, vol. 8, pp. 39659–39671, Feb. 2020, doi: 10.1109/ACCESS.2020.2974058.
[44] K. Elbaz, S. L. Shen, A. N. Zhou, Z. Y. Yin, and H. M. Lyu, "Prediction of disc cutter life during shield tunnelling with AI via incorporation of genetic algorithm into GMDH-type neural network," *Engineering*, to be published.
[45] H. Shi, G. F. Gong, H. Y. Yang, and J. X. Su, "Control model of earth pressure balance for shield tunneling," *Meitan Xuebao/J. China Coal Soc.*, vol. 33, no. 3, pp. 343–346, 2008.
[46] K. Li and C. Shao, "Optimal control for a shield machine subject to multi-point earth pressure balance," *Syst. Sci. Control Eng.*, vol. 3, no. 1, pp. 397–403, Jan. 2015, doi: 10.1080/21642583.2015.1053004.
[47] C. Zhou, H. Xu, L. Ding, L. Wei, and Y. Zhou, "Dynamic prediction for attitude and position in shield tunneling: A deep learning method," *Autom. Construct.*, vol. 105, Sep. 2019, Art. no. 102840, doi: 10.1016/j.autcon.2019.102840.
[48] X. Gao, M. Shi, X. Song, C. Zhang, and H. Zhang, "Recurrent neural networks for real-time prediction of TBM operating parameters," *Autom. Construct.*, vol. 98, pp. 225–235, Feb. 2019, doi: 10.1016/j.autcon.2018.11.013.
[49] K. Cho, B. van Merrienboer, C. Gulcehre, D. Bahdanau, F. Bougares, H. Schwenk, and Y. Bengio, "Learning phrase representations using RNN encoder-decoder for statistical machine translation," 2014, *arXiv:1406.1078*. [Online]. Available: http://arxiv.org/abs/1406.1078
[50] N. Zhang, S.-L. Shen, A. Zhou, and Y.-S. Xu, "Investigation on performance of neural networks using quadratic relative error cost function," *IEEE Access*, vol. 7, pp. 106642–106652, Jul. 2019, doi: 10.1109/ACCESS.2019.2930520.
[51] D. E. Goldberg, *Genetic Algorithms in Search Optimization and Machine Learning*. Menlo Park, CA, USA: Addison-Wesley, 1989.
[52] L. Li, Z. Wen, and Z. Wang, "Outlier detection and correction during the process of groundwater lever monitoring base on Pauta criterion with self-learning and smooth processing," in *Proc. Asian Simulation Conf.*, in Communications in Computer and Information Science, vol. 643, 2016, pp. 497–503, doi: 10.1007/978-981-10-2663-8_51.
[53] D. Ju-Long, "Control problems of grey systems," *Syst. Control Lett.*, vol. 1, no. 5, pp. 288–294, 1982, doi: 10.1016/S0167-6911(82)80025-X.
[54] W. J. M. Rankine, "On the stability of loose earth," *Philos. Trans. Roy. Soc. London*, vol. 147, no. 1, pp. 9–27, 1857.
[55] Z. Zizka and M. Thewes, "Recommendations for face support pressure calculations for shield tunnelling in soft ground," German Tunnelling Committee (ITA-AITES), Cologne, Germany, 2016.

MIN-YU GAO was born in Ya'an, Sichuan, China, in 1996. She received the B.S. degree in civil engineering from Shanghai Jiao Tong University, Shanghai, China, in 2018, where she is currently pursuing the M.S. degree.

Her current research interests include geotechnical and civil engineering, deep-learning techniques, and optimization methods using evolutionary algorithms. Her previous research mainly focused on the microstructure and the stiffness of soil in the small strain state.

Ms. Gao is the Student Chapter President of the Institution of Civil Engineers (ICE), Shanghai Jiao Tong University.

NING ZHANG received the B.Sc. degree in civil engineering from the University of Southeast, in 2013, and the Ph.D. degree in civil engineering from Shanghai Jiao Tong University, China, in 2019.

After he received the Ph.D., he worked in Shantou University as a Research Associate on the automatic control and construction of tunneling. His experience encompasses geotechnical and civil engineering research, deep learning techniques, and constitutive model of materials.

He has also extensive experience in numerical analysis modeling stability of slope, anchor, and tunneling using finite element techniques. He also specializes in optimization of deep learning technique, such as CNN and LSTM.

SHUI-LONG SHEN received the B.Sc. degree in underground space technology and the M.Phil. degree in structural engineering from Tongji University, in 1986 and 1989, respectively, and the Ph.D. degree in geotechnical engineering from Saga University, Japan, in 1998.

After he received the Ph.D., he worked in the Institute of Lowland Technology (ILT), as a Lecturer, from 1998 to 2001. From 2001 to 2003, he worked in the National Institute for Environmental Studies, Tsukuba, Japan. In 2003, he joined the Department of Civil Engineering (DCE), Shanghai Jiao Tong University (SJTU), as a Faculty Member. In 2019, he joined the College of Engineering, Shantou University, as the Dean. He has been keeping collaboration with other international organization, e.g., Saga University, Virginia Tech, The University of Kansas, The University of Hong Kong, the Suranaree University of Technology, Thailand, École Centrale de Nantes, France, the Swinburne University of Technology, and RMIT University, Australia, as a Guest/Visiting/Adjunct Professor. He is currently a Professor.

Dr. Shen also serves as an Editor/Editorial Board Member for four international journals, e.g., *Canadian Geotechnical Journal*, *Geotextiles and Geomembranes*, *Computers and Geotechnics* (Elseveir), *Marine Georesources and Geotechnology* (Taylor and Francis), *Lowland Technology International*, and *Geotechnical Engineering* (SEAGS), and so on and domestic journals, e.g., the *Chinese Journal of Geotechnical Engineering*. From 1998 to 2001, he served as an Associate Editor for the international journal *Lowland Technology International*.

ANNAN ZHOU received the Ph.D. degree in geotechnical engineering from the University of Newcastle, in 2011, with the Australian Endeavor Scholarship. After his graduation, he joined RMIT as a Tenured Lecturer in geotechnical engineering and was promoted to a Senior Lecturer, in 2014 and an Associate Professor, in 2018. He has published more than 70 refereed journal articles with over 1400 citations. His major research area includes constitutive/numerical modeling of multiphase porous media and advanced laboratory testing on unsaturated soils.

The quality of his publications has been recognized by being awarded several international awards, such as the ISSMGE ECR International Best Paper Award, in 2015 and the CGJ Editor's Choice, in 2016. As a Chief Investigator, he has secured several competitive research grants over 1.5 million, including ARC DE, DP, and LP. He was awarded the ARC DECRA Fellowship, in 2012, the AGS Hugh Trollope Medal, in 2014, the CGJ Outstanding Reviewer, in 2016, and the ISSMGE Bright Spark Lecturer Award, in 2018. He has successfully supervised four Ph.D. and two M.Sc. students to their completion. From 2014 to 2016, he was elected to be a RMIT University Research Committee Board Member to represent the ECR academics over the university. Since 2015, he serves as an Editorial Board Member for *Canadian Geotechnical Journal* (NRC), *Underground Space* (Elsevier), and *Advance in Civil Engineering* (Hindawi). He also is invited as an External Reviewer for several national grants, such as ARC, ISF, and NSFC, and numerous flagship journals, such as *Scientific Reports*, *Geotechnique*, and *Computers and Geotechnics*.